ROYAL SOCIETY
OF CHEMISTRY

## PAPER

Check for updates

# Investigation of the adsorption behavior of the anti-cancer drug hydroxyurea on the graphene, BN, AlN, and GaN nanosheets and their doped structures *via* DFT and COSMO calculations

Afiya Akter Piya [ID] *[ab] and A. K. M. Akther Hossain [ID] *[b]

To reduce the direct side effects of chemotherapy, researchers are trying to establish a new approach of a drug-delivery system using nanomaterials. In this study, we investigated graphene and its derivative nanomaterials for their favorable adsorption behavior with the anti-cancer drug hydroxyurea (HU) using DFT calculations. Initially, different pristine and doped graphene and its derivatives were taken into consideration as HU drug carriers. Among them, AlN, GaN, GaN-doped AlN, and AlN-doped GaN nanosheets exhibited favorable adsorption behavior with HU. The HU adsorbed on these four nanosheets with adsorption energies of $-0.92$, $-0.75$, $-0.83$, and $-0.69$ eV, transferring 0.16, 0.032, 0.108, and 0.230 e charges to the nanosheets, respectively, in air medium. In water solvent media, these four nanosheets interacted with HU by $-0.56$, $-0.45$, $-0.58$, and $-0.56$ eV by accepting a significant amount of charge of about 0.125, 0.128, 0.192, and 0.126 e from HU. The dipole moment and COSMO analysis also indicated that these nanosheets, except for GaN-doped AlN, show high asymmetricity and solubility in water solvent media due to the increased values of the dipole moment by two or three times after the adsorption of the HU drug. Quantum molecular descriptors also suggest that the sensitivity and reactivity of the nanosheets are enhanced during the interaction with HU. Therefore, these nanosheets can be used as anti-cancer drug carriers.

## 1. Introduction

Among all the lethal diseases, cancer is the leading cause of death worldwide. With the rapid growth of the global population, the number of new cases has been increasing over the years. A study in 2019 estimated there were about 1 335 100 and 397 583 new cancer cases and cancer-related deaths annually, respectively.[1] One of the key stages in the evaluation of cancer is the loss of control over the cell cycle. Cancer arises when the invading cell proliferation becomes uncontrollable and they spread to other parts of the body.[2] Different kinds of strategies are used for cancer treatment, such as chemotherapy, radiotherapy, and surgery are the common options. Among these options, chemotherapy is the most popular for cancer treatment. There are various therapeutic agents that can be used, known as anti-cancer drugs.[3] Hydroxyurea (HU) is an effective anti-cancer drug that can be taken orally with a short-term toxicity profile in the majority of patients[4] and is used in chemotherapy for cancer treatment. It was first synthesized by

Dresler and Stein in 1869 (ref. 5) and started to be applied as an anti-tumor agent in the 1960s.[6] At present, HU is used to treat leukemia,[7] sickle cell anemia,[8–10] HIV infection,[11] essential thrombocythemia,[12] psoriasis,[13] and polycythemia vera.[14] However, due to its lack of selectivity, it has some adverse effects, such as gastrointestinal disturbance, bone marrow suppression, and dermatological reactions.[6,15]

The main purpose of chemotherapy is to destroy cancerous cells only; however, it also causes damage to normal cells, resulting in some adverse effects, such as fatigue, hair loss, nausea, and vomiting.[16] To minimize the side effects and increase the selectivity of drugs, researchers are trying to implement a way in which nanomaterials can be used as drug carriers. Various nanomaterials are used for drug-delivery purposes, including zero-dimensional (0D), one-dimensional (1D), and two-dimensional (2D) materials.[17–20] Among these, 2D nanomaterials have particularly attracted researchers attention for their promising properties, such as high surface ratio, carrier mobility, and solubility, and exceptional electric and thermal conductivity.[21] Graphene-based 2D nanomaterials have attracted researchers attention owing to their fascinating properties and wide range of applications.[22–26] Experimentally, Guo *et al.* synthesized graphene nanosheets using exfoliated graphite oxide as a precursor.[27] Graphene nanosheets have

*[a]Department of Physics, Mawlana Bhashani Science and Technology University, Tangail, Bangladesh. E-mail: afiya@mbstu.ac.bd*

*[b]Department of Physics, Bangladesh University of Engineering and Technology, Dhaka, Bangladesh. E-mail: akmhossain@phy.buet.ac.bd*

shown great promise due to their wide applications, such as in sensors, emitters, nanoelectronics, nanocomposites, and drug delivery.[28,29] Despite the outstanding characteristics of graphene, one of the primary barriers to employing it for drug delivery is its poor dispersibility in water.[30] Another serious concern related to the potential use of graphene in drug-delivery processes is its intrinsic toxicity.[31–33] Therefore, the toxicity profile should thoroughly be studied before biomedical applications. It has already been recognized that the surface chemistry of nanomaterials plays a crucial role in the biocompatibility and regulated behavior of drugs. Hence, modifications in graphene are necessary to overcome these problems.[34] Also, it has been reported that graphene nanosheets have low interaction with various substances.[35] The doping process is one of the most effective ways to enhance the reactivity of graphene nanosheets.[36] In our previous work, graphene nanosheets were modified by boron (B) and nitrogen (N) atoms to form heterostructures, and it was found that the heteroatoms enhanced the interaction behavior of the nanosheets.[3] Ayoubi-Chianeh *et al.* studied the detection of bendamustine on AlN and Si-doped C nanocones and nanosheets by DFT, and found that AlN nanosheets showed potential as a promising sensor for the bendamustine drug.[37] Very recently in 2023, Ramasamy *et al.* investigated the influence of defects and Si-doping in graphene sheets and claimed that defective and Si-doped graphene are much more suitable as a carrier for drug delivery than pristine sheets.[38] Louis *et al.* also examined heteroatom (B, N, S)-doped graphene quantum dots as a potential drug carrier for isoniazid by DFT and observed that the doped graphene showed a substantial interaction with the drug.[39]

To increase the selectivity of HU as well as its reactivity, pristine graphene (GP), boron nitride (BN), aluminum nitride (AlN), and gallium nitride (GaN) nanosheets, and centrally doped (GP, BN, AlN, and GaN) nanosheets were investigated. The drug-loading mechanism together with the electronic and structural properties of the nanosheets and complexes were investigated in this simulation. The adsorption energy, charge transfer, and energy gap were studied to explore the most compatible carrier for HU. The effects of the solvent were also observed through Conductor-like Screening Model (COSMO) analysis.

## 2. Computational details

All the calculations in the present study were executed using the spin-polarized DFT method in the DMol$^3$ module in both air and water media.[40,41] The generalized gradient approximation (GGA) along with Perdew–Burke–Ernzerhof (PBE) functional were chosen to describe the exchange and correlation.[42] To observe the van der Waals interactions with a long range electron effect, Grimme dispersion-corrected PBE was taken into consideration.[43] Furthermore, in the core treatment, the DFT semi-core pseudopotential with a double-numerical basis set with polarization (DNP) was employed due to its better accuracy than the 6-31G (d, p) basis set in Gaussian.[44,45] In this regard, the DNP basis set can minimize or even eliminate the basis set

superposition error (BSSE). To investigate the solvent effect of the nanosheets and complexes, water medium was used with a dielectric constant of 79.[46] The COSMO technique was used to predict the solvent effect.[47]

In our investigation, the adsorption energy ($E_{Ad}$) of the nanosheets toward the anti-cancer drug HU was calculated by the following equation,[25]

$$E_{Ad} = E_{HU/nanosheets} - E_{nanosheets} - E_{HU} \qquad (1)$$

where, $E_{HU/nanosheets}$, $E_{nanosheets}$, and $E_{HU}$ are the total energies of the complexes, nanosheets, and the HU molecule, respectively.

The frontier molecular orbital (FMO) analysis, *i.e.*, of the highest occupied molecular orbital (HOMO) and lowest unoccupied molecular orbital (LUMO), was performed and the energy gap ($E_g$) between the HOMO and LUMO was computed as follows,

$$E_g = E_{LUMO} - E_{HOMO} \qquad (2)$$

where, $E_{HOMO}$ and $E_{LUMO}$ are the energy of the HOMO and the energy of the LUMO respectively.

Quantum molecular descriptors, such as the chemical potential ($\mu$),[48] global hardness ($\eta$),[49] global softness ($S$),[50] electrophilicity ($\omega$),[51] and nucleophilicity ($\upsilon$) index,[52] were also calculated to predict the reactivity of the nanosheets toward HU by the following equations,

$$\text{Chemical potential, } \mu = -(E_{HOMO} + E_{LUMO})/2 \qquad (3)$$

$$\text{Global hardness, } \eta = (E_{LUMO} - E_{HOMO})/2 \qquad (4)$$

$$\text{Global softness, } S = 1/2\eta \qquad (5)$$

$$\text{Electrophilicity index, } \omega = \mu^2/2\eta \qquad (6)$$

$$\text{Nucleophilicity index. } \upsilon = 1/\omega \qquad (7)$$

## 3. Results and discussion

### 3.1 Geometry of optimized nanosheets

In this project, we chose pristine graphene, boron nitride (BN), aluminum nitride (AlN), and gallium nitride (GaN) nanosheets and their doped nanosheets. Four pristine and twelve doped nanosheets were taken into consideration as drug carriers for HU molecules. The pristine GP nanosheet was modified by hexagonally doping BN, AlN, and GaN at the central position. Similarly, the other nanosheets were also modified and all the nanosheets were optimized at the ground state, as shown in Fig. 1. All the nanosheets consisted of 16 hexagons with 66 atoms. In this study, the pristine graphene nanosheet comprised 48 carbon atoms and at the edge, the carbon atoms were passivated with hydrogen atoms to increase its stability. The average bond length of C–C in GP was 1.413 Å, which was consistent with a previous study.[53] The bond length of C–H was 1.093 Å and was in good agreement with our prior study.[2] In
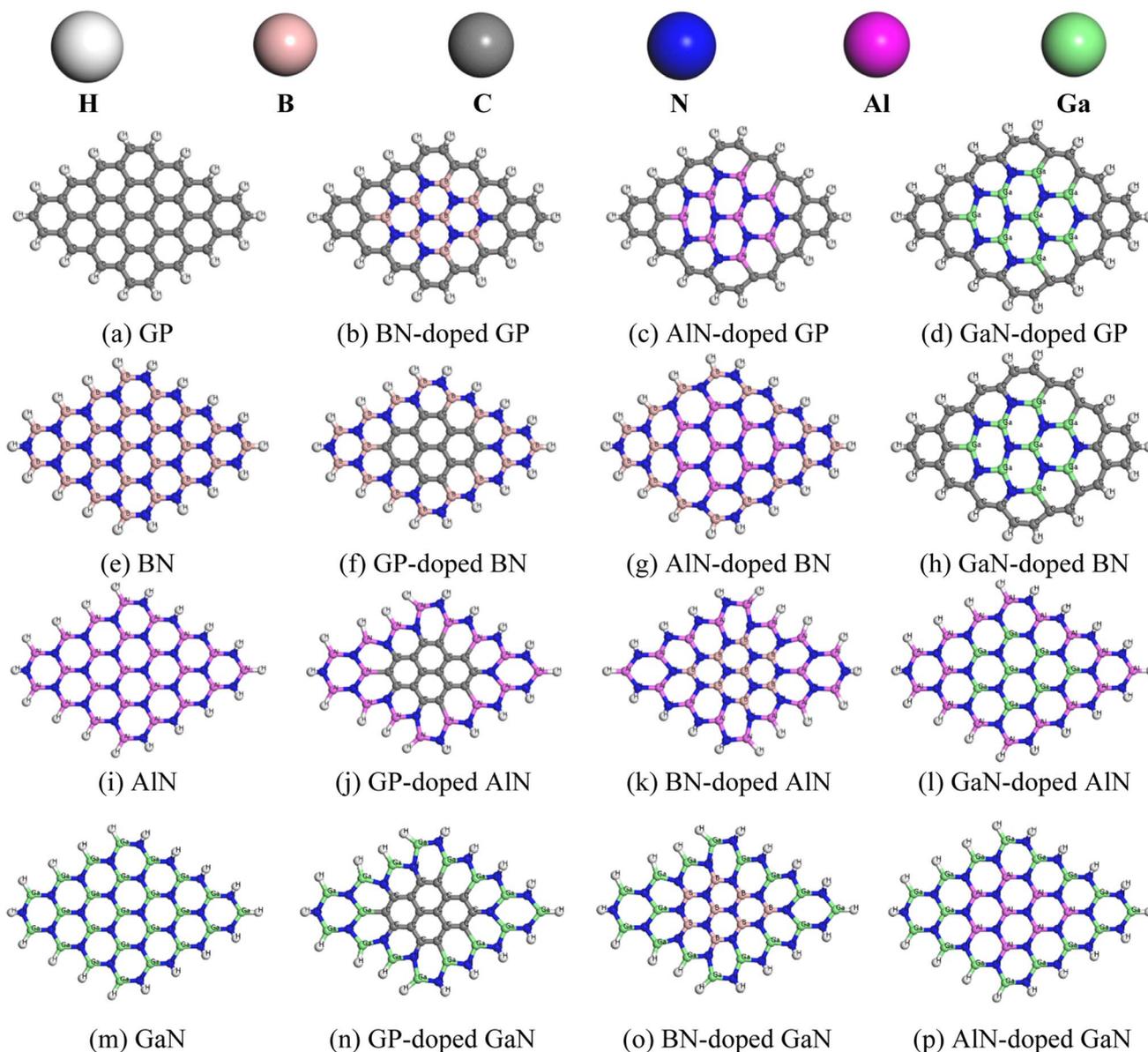
Fig. 1 Top view of the optimized pristine (a, e, i and m) and doped nanosheets (b–d, f–h, j–l, n–p), in which the white, gray, brown, blue, pink, and green color spheres indicate hydrogen, carbon, boron, nitrogen, aluminum, and gallium atoms, respectively.

addition, the bond angles of C–C–C and C–C–H in graphene were 120.09° and 118.85°. When GP was doped centrally by BN, AlN, or GaN (doped concentration of about 25%), the modified nanosheets remained in a planer form with average bond lengths of B–N, Al–N, and Ga–N of 1.45, 1.74, and 1.75 Å. The average bond length of B–N in BN was 1.46 Å, whereas a previous study found a bond length of 1.44 Å.[2] After doping by GP, AlN, or GaN, the bond lengths of C–C, Al–N, and Ga–N were 1.42, 1.74, and 1.77 Å. Moreover, the average bond lengths of Al–N in AlN and Ga–N in GaN were found to be 1.81 and 1.84 Å, which were in good agreement with previous work.[2] Fig. 2 shows the DOS and PDOS spectra of the nanosheets, confirming that the nanosheets did not show the magnetic behavior due to their symmetry of their spin-up and spin-down DOS.

### 3.2 Adsorption of HU on the GP and the BN-, AlN-, and GaN-doped graphene

To investigate the adsorption phenomenon of HU on the pristine GP and doped (BN, AlN, and GaN) GP, the HU drug was adsorbed at the middle of the nanosheets in a parallel configuration. Previous studies suggested that drug molecules were favorably adsorbed on the nanosheets when placed in a parallel way.[54,55] Thus, we have placed HU in a parallel way on the nanosheets and all the complexes were then optimized. After optimization, we found that among the 16 complexes, 8 complexes showed high stability, as shown in Fig. 3, while the other complexes were highly deformed. The adsorption energies were calculated by using eqn (1) (Table 1) and a negative interaction energy was found, which implied an attractive and
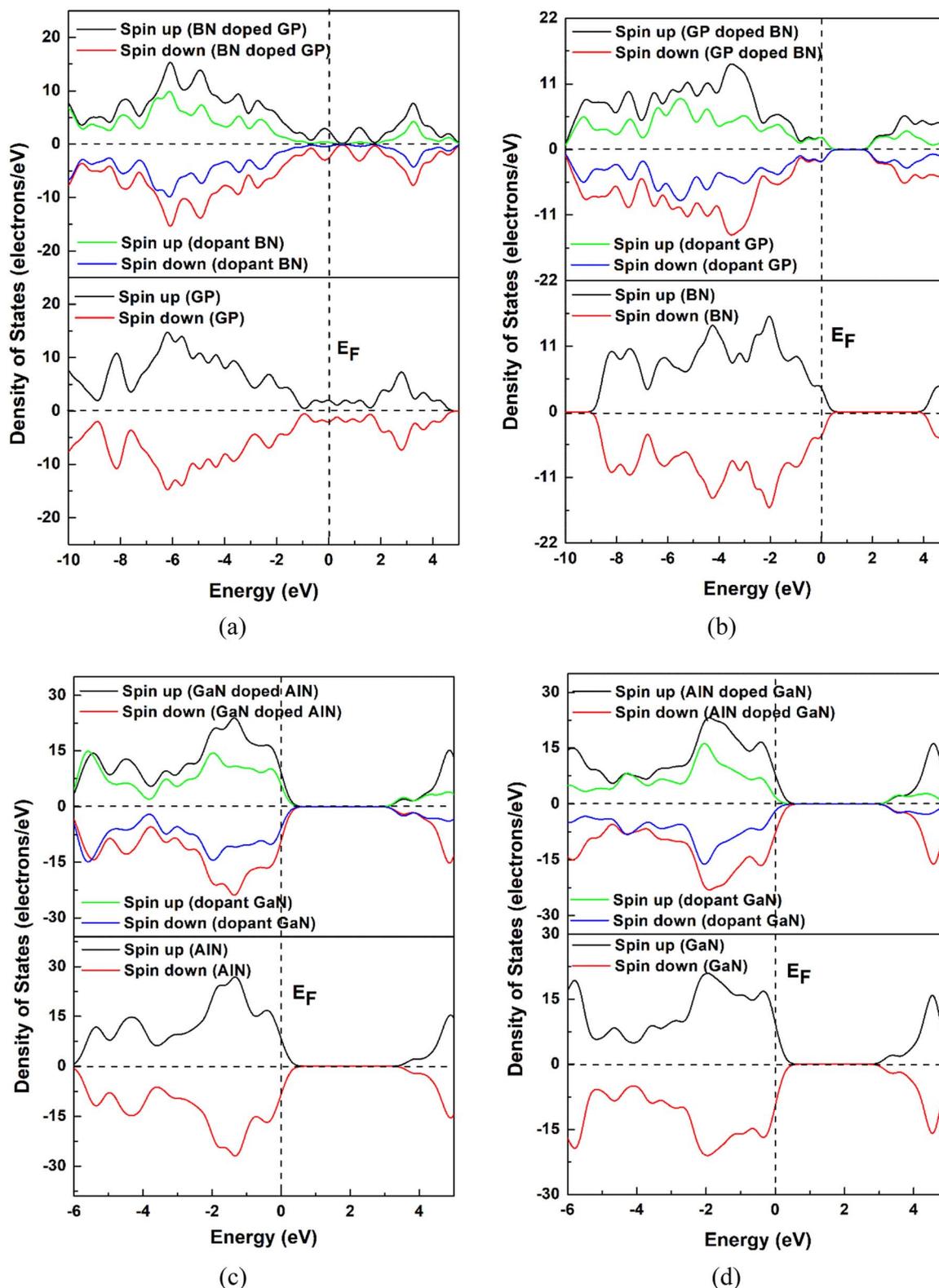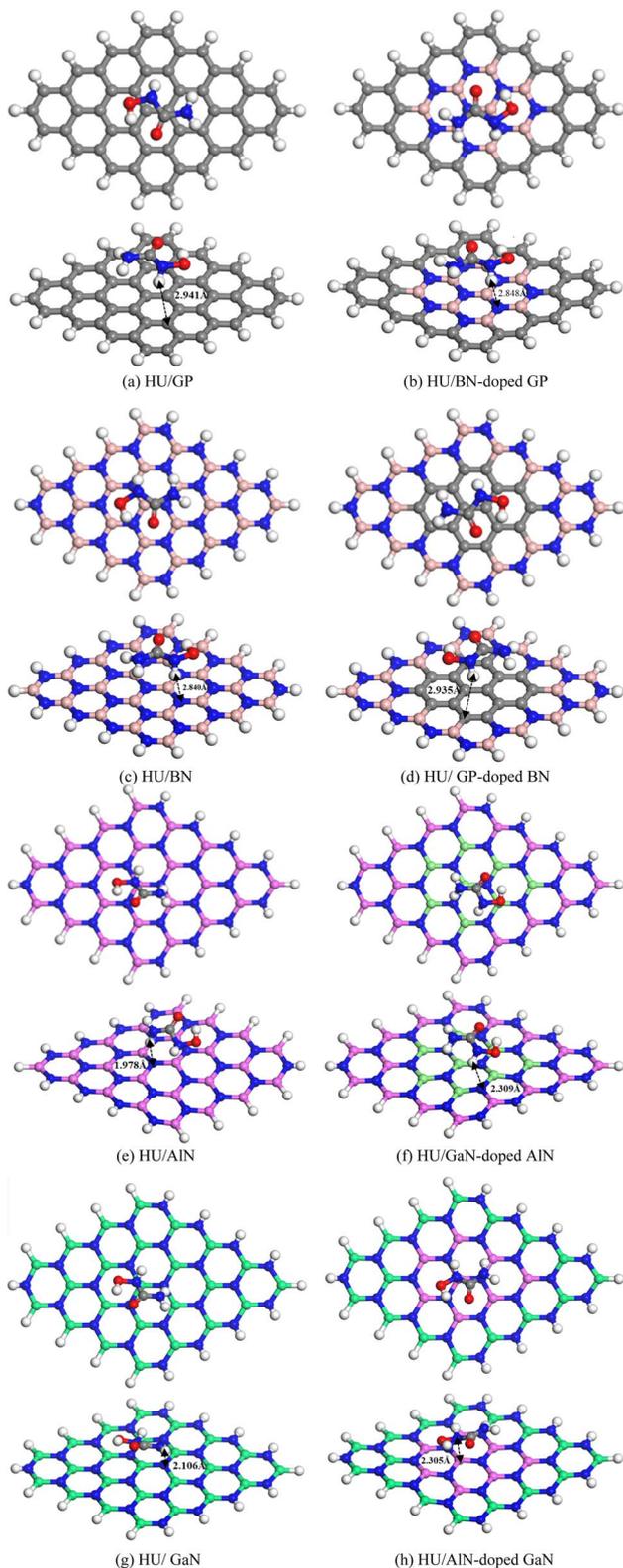
**Fig. 2** DOS and PDOS spectra of the pristine and doped nanosheets (a) GP and BN-doped GP, (b) BN and GP-doped BN, (c) AlN and GaN-doped AlN and (d) GaN and AlN-doped GaN.

exothermic interaction with HU. The obtained values were −0.49, −0.54, −9.94, and −9.89 eV for the pristine and BN-, AlN-, and GaN-doped GP, respectively. Although the AlN- and GaN-doped GP showed a very high interaction phenomenon with the HU drug, these nanosheets were highly deformed, and thus showed a very low structural stability with HU drug. They

**Table 1** Calculated adsorption energy ($E_{Ad}$) in (eV), charge transfer ($Q$) in (e), and minimum interaction distance ($d$) in (Å)

| Structures | Air media | | | Water media | | |
|---|---|---|---|---|---|---|
| | $E_{Ad}$ (eV) | $Q$ (e) | $d$ (Å) | $E_{Ad}$ (eV) | $Q$ (e) | $d$ (Å) |
| HU/GP | −0.49 | −0.035 | 3.329 | −0.35 | 0.033 | 2.948 |
| HU/BN-doped GP | −0.54 | 0.042 | 3.291 | −0.36 | 0.031 | 2.991 |
| HU/BN | −0.45 | 0.003 | 3.334 | −0.31 | 0.018 | 2.893 |
| HU/GP-doped BN | −0.46 | −0.043 | 3.344 | −0.32 | 0.026 | 2.959 |
| HU/AlN | −0.92 | 0.16 | 2.199 | −0.56 | 0.125 | 2.292 |
| HU/GaN-doped AlN | −0.75 | 0.032 | 3.218 | −0.45 | 0.128 | 2.204 |
| HU/GaN | −0.83 | 0.108 | 2.319 | −0.58 | 0.192 | 2.324 |
| HU/AlN-doped GaN | −0.69 | 0.23 | 2.305 | −0.56 | 0.126 | 2.268 |



**Fig. 3** Top and side views of the stable optimized complexes (a) HU/GP, (b) HU/BN-doped GP, (c) HU/BN, (d) HU/GP-doped BN, (e) HU/AlN, (f) HU/GaN-doped AlN, (g) HU/GaN and (h) HU/AlN-doped GaN.

formed clusters with HU drug. Therefore, the AlN- and GaN-doped GP were not suitable as drug carriers due to their very high interaction energy and high structural deformation. Again we also examined the adsorption performance of BN nanosheet and GP-, AlN-, and GaN-doped BN nanosheets for HU drug. Similarly, HU drug was adsorbed on the nanosheets and it was found that the AlN- and GaN-doped BN nanosheets are not suitable as HU drug carriers due to the very large adsorption energies (−6.22 and −7.02 eV for the AlN- and GaN-doped BN nanosheets) and high structural deformation. The BN- and GP-doped BN nanosheets showed almost similar interaction behaviors with HU. HU drug was adsorbed on these nanosheets with −0.45 and −0.46 eV energies, respectively. Furthermore, pristine AlN and GP-, BN-, and GaN-doped AlN nanosheets were taken into consideration as HU drug carriers, and we have found that HU drug was adsorbed on these nanosheets with adsorption energies of −0.92, −5.52, −4.71, and −0.75 eV, respectively. In this case, the pristine AlN and GaN-doped AlN showed very suitable interaction behaviors in low-range chemisorption interactions as drug carriers. The pristine GaN and GP-, BN-, and AlN-doped GaN nanosheets were also investigated and it was found that they had adsorption energies of −0.83, −4.93, −4.67, and −0.69 eV, respectively. In this case, the pristine GaN and AlN-doped GaN exhibited favorable interaction energy with HU drug. Therefore, among the 16 nanosheets, four nanosheets, namely AlN, GaN-doped AlN, GaN, and AlN-doped GaN, showed favorable interaction behaviors in the range of −0.69 to −0.92 eV. During the interaction with HU, Mulliken charge analysis was considered and calculated by the following equation,

$$\text{Charge transfer, } Q = Q_a(\text{HU}) - Q_b(\text{HU}) \qquad (8)$$

where, $Q_a$ (HU) and $Q_b$ (HU) are the net charge on HU after and before adsorption on the nanosheets, respectively. According to the Mulliken charge analysis, during the interaction of HU on these four nanosheets, a significant amount of charge of about 0.16e, 0.032e, 0.108e, and 0.23e was transferred to the AlN, GaN-doped AlN, GaN, and AlN-doped GaN from HU drug.

Frontier molecular orbital (FMO) as well as energy gap ($E_g$) analyses were performed and the results are tabulated in Table 2. Fig. 4 shows the FMO maps of the stable complexes of

**Table 2** HOMO energy ($E_{HOMO}$), LUMO energy ($E_{LUMO}$), HOMO–LUMO energy gap ($E_g$) in (eV), change in energy gap (% $\Delta E_g$), dipole moment (D.M) in Debye, and solvation energy ($E_{solv}$) in eV of the complexes

| Structures | Air media | | | | Water media | | | | |
|---|---|---|---|---|---|---|---|---|---|
| | $E_{HOMO}$ | $E_{LUMO}$ | $E_g$ | D.M | $E_{HOMO}$ | $E_{LUMO}$ | $E_g$ | D.M | $E_{solv}$ |
| GP | −4.256 | −3.618 | 0.638 | 0 | −4.515 | −3.881 | 0.634 | 0 | 1.7 |
| HU/GP | −4.346 | −3.71 | 0.636 | 2.82 | −4.509 | −3.877 | 0.632 | 5.16 | 1.38 |
| BN-doped GP | −4.395 | −3.359 | 1.036 | 1.82 | −4.613 | −3.55 | 1.063 | 4.38 | 1.03 |
| HU/BN-doped GP | −4.386 | −3.354 | 1.032 | 1.94 | −4.6 | −3.54 | 1.06 | 4.21 | 0.74 |
| BN | −5.843 | −1.455 | 4.388 | 5.78 | −5.864 | −1.704 | 4.16 | 7.95 | −0.56 |
| HU/BN | −5.358 | −1.475 | 3.883 | 8.38 | −5.781 | −1.706 | 4.075 | 12.3 | −0.87 |
| GP-doped BN | −4.686 | −2.496 | 2.19 | 2.64 | −5.011 | −2.815 | 2.196 | 2.93 | 0.11 |
| HU/GP-doped BN | −4.799 | −2.647 | 2.152 | 2.81 | −4.998 | −2.819 | 2.179 | 3.60 | −0.22 |
| AlN | −5.525 | −1.682 | 3.843 | 4.49 | −5.438 | −1.607 | 3.831 | 6.62 | −0.29 |
| HU/AlN | −5.601 | −1.745 | 3.856 | 7.82 | −5.382 | −1.508 | 3.874 | 12.51 | −0.40 |
| GaN-doped AlN | −5.559 | −2.024 | 3.535 | 4.58 | −5.485 | −1.982 | 3.503 | 6.79 | −0.37 |
| HU/GaN-doped AlN | −5.488 | −2.151 | 3.337 | 2.18 | −5.44 | −1.951 | 3.489 | 2.97 | −0.55 |
| GaN | −5.446 | −2.088 | 3.358 | 2.74 | −5.622 | −2.213 | 3.409 | 3.46 | −0.57 |
| HU/GaN | −5.491 | −2.125 | 3.366 | 5.59 | −5.603 | −2.149 | 3.454 | 9.34 | −0.79 |
| AlN-doped GaN | −5.418 | −1.88 | 3.538 | 2.84 | −5.563 | −1.963 | 3.6 | 3.68 | −0.4 |
| HU/AlN-doped GaN | −5.402 | −1.998 | 3.404 | 5.91 | −5.53 | −1.908 | 3.622 | 10.56 | −0.74 |

the HU/nanosheets. As AlN, GaN-doped AlN, GaN, and AlN-doped GaN showed favorable interactions with HU, we discuss the FMO analyses of these nanosheets in this section. The HOMO levels were located at −5.525, −5.559, −5.446, and −5.418 eV and LUMO levels at −1.682, −2.024, −2.088, and −1.88 eV for AlN, GaN-doped AlN, GaN, and AlN-doped GaN nanosheets. After adsorption of HU on the nanosheets, the HOMO and LUMO levels varied. For example, for GaN-doped AlN and AlN-doped GaN, the HOMO levels were reduced from −5.559 and −5.418 to −5.488 and −5.402 eV while the LUMO levels increased from −2.024 and −1.88 eV to −2.151 and −1.998 eV, respectively. The HOMO and LUMO gap, *i.e.*, the energy gap, was also calculated and it was found that the energy gap was reduced from 3.535 to 3.337 eV and 3.538 to 3.404 eV for GaN-doped AlN and AlN-doped GaN nanosheets, respectively. The conductivity ($\sigma$) of these nanosheets was exponentially enhanced due to the reduction in the energy gap ($E_g$) and maintained the following relation,[56]

$$\sigma \propto e^{\left(\frac{-E_g}{2KT}\right)} \tag{9}$$

where, $K$ is Boltzmann's constant = $1.380 \times 10^{-23}$ m$^2$ kg$^{-2}$ k$^{-1}$.

### 3.3 Dipole moment

The dipole moment is one of the key terms to study the interaction between an absorbent and drug. It is also well known that the dipole moment can also explain the asymmetric charge distribution and reactivity of a system. The non-polar nature of a molecule is shown when the value of the dipole moment is zero.[57,58] The dipole moments of the different nanosheets and complexes are tabulated in Table 2. A high value of dipole moment indicates more reactivity and solubility in polar solvents. After the adsorption of HU drug on the nanosheets, the value of dipole moment increased, indicating that the HU drug can move easily in biochemical systems. The dipole

moments of our pristine GP, BN-doped GP, BN, GP-doped BN, AlN, GaN-doped AlN, GaN, and AlN-doped GaN nanosheets were 0, 1.82, 5.78, 2.64, 4.49, 4.58, 2.74, and 2.84 D before the adsorption process, respectively. After HU interacted with the nanosheets, the dipole moments rose, specifically to 2.82, 1.94, 8.38, 2.81, 7.82, 5.59, and 5.91 D, respectively, except for the GaN-doped AlN nanosheets. The above increases of the dipole moments enhanced the solubility of the nanosheets in polar media. According to the charge-transfer analysis as well as dipole moment analysis, among these complexes, HU/AlN, HU/GaN, and HU/AlN-doped GaN showed the highest reactivity. Interestingly, these three complexes also showed more reactivity in water solvent media due to their high dipole moment in the media, with about a 2 or 3 times enhanced dipole moment of the three nanosheets after adsorption of HU drug. The dipole moments of AlN, GaN, and AlN-doped GaN nanosheets in water solvent media were 6.62, 3.46, and 3.68 D, but after interaction with HU drug, the dipole moments increased to 12.51, 9.34, and 10.56 D, respectively. A bar diagram comparing the dipole moments is shown in Fig. 5 in air and water media.

### 3.4 Drug release

The drug-release mechanism is another vital element in a drug-delivery system. In this case, we obtained the drug desorption times from the nanosheets by using the van't Hoff–Arrhenius and transition-state theory as follows,

$$\tau = \frac{1}{v_o} \exp\left(\frac{-E_{ads}}{K_B T}\right) \tag{10}$$

where $T$ is the temperature in K, in which case here we calculated the desorption time by considering three temperatures, namely at room temperature (298 K), normal body temperature (310 K), and cancer tissue temperature (315 K); $v_o$ is the attempt frequency ($10^{12}$ Hz); and $K_B$ is Boltzmann's constant. The desorption time exponentially depends on the adsorption
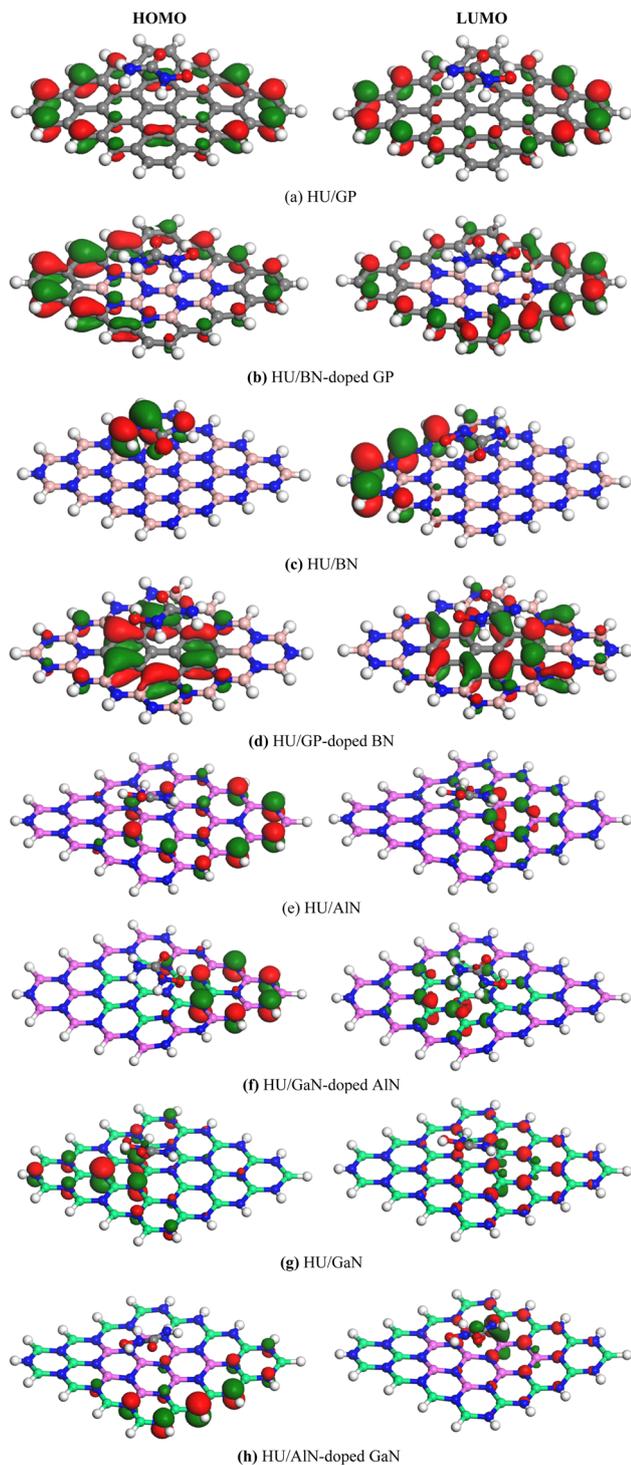
**Fig. 4** HOMO and LUMO maps of the stable (a) HU/GP, (b) HU/BN-doped GP, (c) HU/BN, (d) HU/GP-doped BN, (e) HU/AlN, (f) HU/GaN-doped AlN, (g) HU/GaN and (h) HU/AlN-doped GaN complexes.

energy, which implies that a higher adsorption energy will suffer from a longer desorption time. Among our proposed nanosheets, the AlN, GaN-doped AlN, GaN, and AlN-doped GaN nanosheets show favorable interaction energies in the range from −0.69 to −0.92 eV. The desorption of HU drug from the

AlN, GaN-doped AlN, GaN, and AlN-doped GaN nanosheets took 391.47, 0.75, 17.6, and 0.10 s in air media and 0.00067, 0.000015, 0.0016, and 0.00086 s in water media at the cancer tissue temperature (Table 3). These desorption times were sufficient for the desorption of HU from the nanosheets, which was confirmed from previous studies.

### 3.5 Quantum molecular descriptors

Quantum molecular descriptors, such as the chemical potential ($\mu$), global hardness ($\eta$), global softness ($S$), and electrophilicity index ($\omega$), have been investigated to predict the reactivity of the nanosheets toward HU drug.[59] The descriptors were from the ionization potential and electron affinity, where in practice the ionization potential and electron affinity are nothing but the negative energy of the HOMO and LUMO. The calculated values are tabulated in Table 4. The chemical potential indicates the tendency for an electron to escape from an equilibrium position. The calculated values of the chemical potentials of the nanosheets were enhanced after the adsorption of HU drug, except for the BN nanosheet, which indicated that the reactivity of the nanosheets increased towards the HU drug. The calculated chemical potentials for the GP, BN-doped GP, GP-doped BN, AlN, GaN-doped AlN, GaN, and AlN-doped GaN nanosheets were −3.94, −3.87, −3.59, −3.60, −3.79, −3.77, and −3.65 eV, respectively. After adsorption of HU on the nanosheets, the values were enhanced to −4.03, −3.87, −3.72, −3.67, −3.82, −3.81, and −3.70 eV, respectively. The global hardness and softness are another two important parameters that also help define the reactivity of complexes. In the presence of an external electric field, the resistance to deform a structure indicates the values of the global hardness. Higher values of global hardness indicate a higher strength of the nanosheets in the presence of the electric field. The global softness has an opposite relation with the global hardness. Higher values of global softness imply a high reactivity of the nanosheets. In our observation, all the nanosheets, except AlN and GaN, exhibited reactivity after adsorption of HU drug as confirmed by the decreasing values of the global hardness and increasing values of the global softness in the gaseous as well as water solvent medium, as shown in Table 4. The electrophilicity index was also calculated to investigate the electrophilic power, *i.e.*, the ability of the nanosheets to accept electrons.[60] Our calculated values show that, except for AlN and GaN, all the nanosheets displayed high electrophilicity after interaction with HU drug. Furthermore, higher values of the dipole moment of the nanosheets, except for GaN-doped AlN, in the water media were found compared with the gas phase, which confirmed that the AlN, GaN-doped AlN, GaN, and AlN-doped GaN nanosheets have potential for use as drug carriers for HU in water solvent medium.

### 3.6 Solvent effect

To investigate the solvent effect on the complexes, the solvation energy, adsorption energy, electronic properties, and dipole moment in water media were calculated and are shown in Tables 3 and 4. The solvation energy was calculated by the
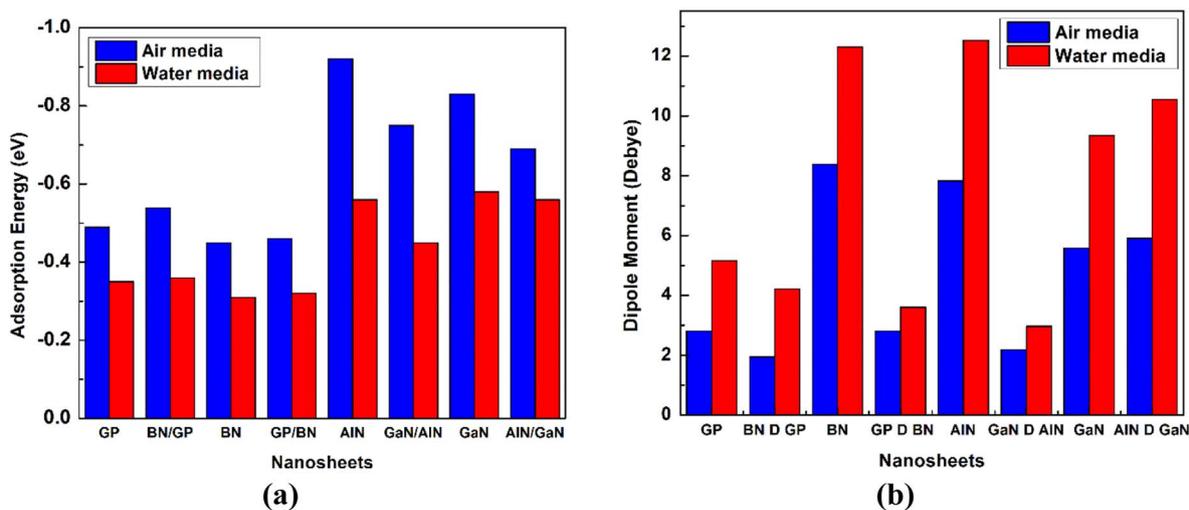
Fig. 5 Comparison of the (a) adsorption energy and (b) dipole moment between the cases in the air and in water media.

Table 3 HU drug–release time in gaseous and water media at room temperature (298 K), body temperature (310 K), and cancer tissue temperature (315 K)

| Structures | Air media | | | Water media | | |
|---|---|---|---|---|---|---|
| | 298 K | 310 K | 315 K | 298 K | 310 K | 315 K |
| HU/GP | $2.3 \times 10^{-4}$ | $1.1 \times 10^{-4}$ | $8.24 \times 10^{-5}$ | $7.04 \times 10^{-7}$ | $4.18 \times 10^{-7}$ | $3.41 \times 10^{-7}$ |
| HU/BN-doped GP | $1.1 \times 10^{-3}$ | $5.2 \times 10^{-4}$ | $3.8 \times 10^{-4}$ | $9.62 \times 10^{-7}$ | $5.64 \times 10^{-7}$ | $4.57 \times 10^{-5}$ |
| HU/BN | $5.26 \times 10^{-5}$ | $2.64 \times 10^{-5}$ | $2.01 \times 10^{-5}$ | $1.49 \times 10^{-7}$ | $9.4 \times 10^{-8}$ | $7.83 \times 10^{-8}$ |
| HU/GP-doped BN | $5.75 \times 10^{-5}$ | $2.88 \times 10^{-5}$ | $2.19 \times 10^{-5}$ | $2.35 \times 10^{-7}$ | $1.45 \times 10^{-7}$ | $1.2 \times 10^{-7}$ |
| HU/AlN | 2661.76 | 673.08 | 391.47 | $2.1 \times 10^{-3}$ | $9.3 \times 10^{-4}$ | $6.7 \times 10^{-4}$ |
| HU/GaN-doped AlN | 3.59 | 1.17 | 0.75 | $3.88 \times 10^{-5}$ | $1.97 \times 10^{-5}$ | $1.51 \times 10^{-5}$ |
| HU/GaN | 100.25 | 28.78 | 17.6 | $5.4 \times 10^{-3}$ | $2.27 \times 10^{-3}$ | $1.6 \times 10^{-3}$ |
| HU/AlN-doped GaN | 0.44 | 0.16 | 0.10 | $2.78 \times 10^{-3}$ | $1.2 \times 10^{-3}$ | $8.61 \times 10^{-4}$ |

Table 4 Values of the chemical potential ($\mu$), global hardness ($\eta$), electrophilicity index ($\omega$) in unit eV, nucleophilicity index $v$, and global softness ($S$) in unit eV$^{-1}$ in gaseous and solvent media

| Structure | Air media | | | | | Water media | | | | |
|---|---|---|---|---|---|---|---|---|---|---|
| | $\mu$ (eV) | $\eta$ (eV) | $S$ (eV$^{-1}$) | $\omega$ (eV) | $v$ (eV$^{-1}$) | $\mu$ (eV) | $\eta$ (eV) | $S$ (eV$^{-1}$) | $\omega$ (eV) | $v$ (eV$^{-1}$) |
| GP | −3.94 | 0.319 | 1.567 | 24.29 | 0.041 | −4.198 | 0.317 | 1.577 | 27.796 | 0.036 |
| HU/GP | −4.03 | 0.318 | 1.572 | 25.51 | 0.039 | −4.193 | 0.316 | 1.582 | 27.818 | 0.036 |
| BN-doped GP | −3.87 | 0.518 | 0.965 | 14.51 | 0.069 | −4.082 | 0.532 | 0.941 | 15.671 | 0.064 |
| HU/BN-doped GP | −3.87 | 0.516 | 0.969 | 14.52 | 0.069 | −4.070 | 0.530 | 0.943 | 15.627 | 0.064 |
| BN | −3.65 | 2.194 | 0.228 | 3.03 | 0.330 | −3.784 | 2.080 | 0.240 | 3.442 | 0.291 |
| HU/BN | −3.42 | 1.942 | 0.258 | 3.01 | 0.332 | −3.744 | 2.038 | 0.245 | 3.439 | 0.291 |
| GP-doped BN | −3.59 | 1.095 | 0.457 | 5.89 | 0.170 | −3.913 | 1.098 | 0.455 | 6.972 | 0.143 |
| HU/GP-doped BN | −3.72 | 1.076 | 0.465 | 6.44 | 0.155 | −3.909 | 1.090 | 0.459 | 7.011 | 0.143 |
| AlN | −3.60 | 1.922 | 0.260 | 3.38 | 0.296 | −3.523 | 1.916 | 0.261 | 3.239 | 0.309 |
| HU/AlN | −3.67 | 1.928 | 0.259 | 3.50 | 0.286 | −3.445 | 1.937 | 0.258 | 3.063 | 0.326 |
| GaN-doped AlN | −3.79 | 1.766 | 0.283 | 4.07 | 0.246 | −3.734 | 1.752 | 0.285 | 3.979 | 0.251 |
| HU/GaN-doped AlN | −3.82 | 1.669 | 0.299 | 4.37 | 0.229 | −3.696 | 1.745 | 0.287 | 3.914 | 0.255 |
| GaN | −3.77 | 1.679 | 0.298 | 4.23 | 0.237 | −3.918 | 1.705 | 0.293 | 4.501 | 0.222 |
| HU/GaN | −3.81 | 1.683 | 0.297 | 4.31 | 0.232 | −3.876 | 1.727 | 0.290 | 4.350 | 0.229 |
| AlN-doped GaN | −3.65 | 1.769 | 0.283 | 3.76 | 0.266 | −3.763 | 1.800 | 0.278 | 3.933 | 0.254 |
| HU/AlN-doped GaN | −3.70 | 1.702 | 0.294 | 4.02 | 0.249 | −3.719 | 1.811 | 0.277 | 3.819 | 0.262 |

difference between the total energy of the complex in the water and air media, as shown below,

$$E_{solv} = E_{water} - E_{air}$$

The negative values of solvation energy of the complexes indicated their stability and solubility in the solvent media. In our solvation energy calculations, among the eight nanosheets, GP, BN-doped GP, and GP-doped BN did not show stability in the solvent media due to their positive values of solvation energy, while the other nanosheets showed good stability in water media. After adsorption of the HU on the nanosheets, the solvation energies became more negative, which implied their high stability in the water media. The calculated values were −0.56, −0.29, −0.37, 0.57, and −0.4 eV for the BN, AlN, GaN-doped AlN, GaN, and AlN-doped GaN nanosheets. After the interaction of HU with these nanosheets, the solvation energies were enhanced to −0.87, −0.40, −0.55, −0.79, and −0.74 eV,

respectively. The adsorption energies in the water media were also calculated and confirm the attractive interaction between the HU and nanosheets due to their negative adsorption energies. The calculated values of the adsorption energies were −0.56, −0.45, −0.58, and −0.56 eV for the AlN, GaN-doped AlN, GaN, and AlN-doped GaN nanosheets, respectively. During the interaction, the HU drug loses 0.125, 0.128, 0.192, and 0.126 e to the nanosheets, respectively. The drug was adsorbed by keeping 2.292, 2.204, 2.324, and 2.268 Å distance from the nanosheets.

To gain more insights into the solvent effect, COSMO surface analysis of our complexes was performed. The visualization of the COSMO surfaces, as shown in Fig. 6, shows the polar and non-polar regions of the complexes. In this COSMO surface, the red portion implies a hydrogen bond donor (HBD) region, which is the positively charged region. On the other hand, the blue portion indicates the hydrogen bond acceptor (HBA) region, which is the negatively charged region of the complexes. Also, the yellowish green portion implies a neutral region as
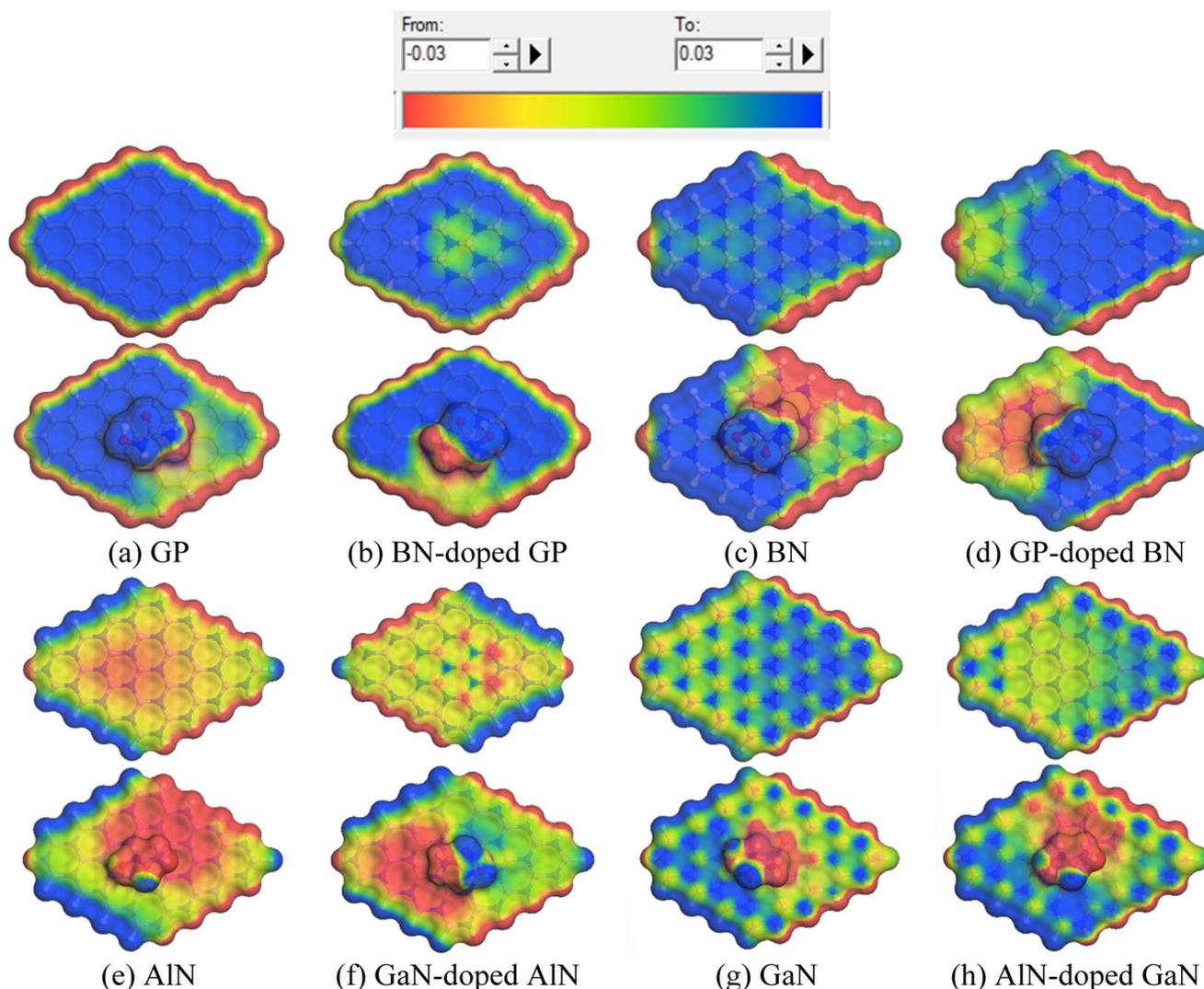


**Fig. 6** Front views of the COSMO surfaces of the (a) GP, (b) BN-doped GP, (c) BN, (d) GP-doped BN, (e) AlN, (f) GaN-doped AlN, (g) GaN and (h) AlN-doped GaN before and after adsorption of HU.

well as non-polar region of the complexes. In our investigation, it was clearly seen that after adsorption of the HU on the nanosheets, especially on the AlN, GaN-doped AlN, GaN, and AlN-doped GaN nanosheets, the HBD region appeared large, implying the high polarity of the complexes in the water solvent media.

## 4. Conclusions

Anti-cancer drug delivery by nanomaterials has been a widely studied topic in recent years to reduce the direct side effects of chemotherapy in cancer treatment. The challenging issue in this case is to find a suitable drug carrier with favorable range adsorption behavior with a short desorption time at cancerous cells. In this study, DFT calculations with the GGA-PBE functional were employed to investigate graphene and its derivative nanomaterials that might show a favorable adsorption behavior with the HU anti-cancer drug. Initially, different pristine and doped graphene and its derivatives were taken into consideration as HU carriers. Among these, AlN, GaN, GaN-doped AlN, and AlN-doped GaN nanosheets exhibited favorable adsorption behavior with HU. The HU adsorbed on the four nanosheets by −0.92, −0.75, −0.83, and −0.69 eV adsorption energies and with transferring 0.16, 0.032, 0.108, and 0.230 e charges to the nanosheets, respectively, in air media. In water solvent media, these four nanosheets interacted with HU by −0.56, −0.45, −0.58, and −0.56 eV and by accepting a significant amount of charge of about 0.125, 0.128, 0.192, and 0.126 e from the HU. Dipole moment and COSMO analyses also proved that the four nanosheets, except for GaN-doped AlN, showed high asymmetry and solubility in water solvent media. The calculated dipole moments of the AlN, GaN, and AlN-doped GaN nanosheets in water solvent media were 6.62, 3.46, and 3.68 D, but after interaction with HU drug, the dipole moments increased to 12.51, 9.34, and 10.56 D, respectively. Furthermore, the quantum molecular descriptors also suggested that the sensitivity and reactivity of the nanosheets were enhanced during the interaction with HU. Therefore, these four nanosheets may have potential to be used as HU carriers.

## Author contributions

Afiya Akter Piya: writing – original draft, data curation; A. K. M. Akther Hossain: review & editing, supervision.

## Conflicts of interest

The authors declare that they have no known competing financial interests or personal relationships that could have appeared to influence the work reported in this paper.

## Acknowledgements

## References

1 L. You, Z. Lv, C. Li, W. Ye, Y. Zhou, J. Jin and Q. Han, *Worldwide cancer statistics of adolescents and young adults in 2019: a systematic analysis of the Global Burden of Disease Study 2019*, ESMO Open, 2021, DOI: **10.1016/j.esmoop.2021.100255**.

2 T. Ahmed, M. Aminur Rahman, R. Islam, A. Akter Piya and S. Ud Daula Shamim, Unravelling the adsorption performance of BN, AlN, GaN and InN 2D nanosheets towards the ciclopirox, 5-fluorouracil and nitrosourea for anticancer drug delivery motive: A DFT-D with QTAIM, PCM and COSMO investigations, *Comput. Theor. Chem.*, 2022, **1214**, 113797, DOI: **10.1016/J.COMPTC.2022.113797**.

3 K. N. Munny, T. Ahmed, A. A. Piya and S. U. D. Shamim, Exploring the adsorption performance of doped graphene quantum dots as anticancer drug carriers for cisplatin by DFT, PCM, and COSMO approaches, *Struct. Chem.*, 2023, 1–17, DOI: **10.1007/S11224-023-02150-Y/METRICS**.

4 K. Madaan, D. Kaushik and T. Verma, Hydroxyurea: A key player in cancer chemotherapy, *Expert Rev. Anticancer Ther.*, 2012, **12**, 19–29, DOI: **10.1586/era.11.175**.

5 W. F. C. Dresler and R. Stein, Ueber den Hydroxylharnstoff, *Justus Liebigs Ann. Chem.*, 1869, DOI: **10.1002/jlac.18691500212**.

6 N. Saban and M. Bujak, Hydroxyurea and hydroxamic acid derivatives as antitumor drugs, *Cancer Chemother. Pharmacol.*, 2009, DOI: **10.1007/s00280-009-0991-z**.

7 E. J. Verspohl, E. Mutschler and H. Derendorf, Drug Actions. Basic Principles and Therapeutic Aspects, Medpharm Scientific Publishers, CRC Press Stuttgart, 1995, 799, 516, DM 124, Pharm, Unserer Zeit, 1996, DOI: **10.1002/pauz.19960250618**.

8 S. Charache, G. J. Dover, M. A. Moyer and J. W. Moore, Hydroxyurea-induced augmentation of fetal hemoglobin production in patients with sickle cell anemia, *Blood*, 1987, **69**, 109–116, DOI: **10.1182/blood.v69.1.109.bloodjournal691109**.

9 C. Samuel, T. Michael, M. Richard, D. George, B. Franca, E. Susan, M. Robert and B. Duane, Effect of hydroxyurea on the frequency of painful crises in sickle cell anemia. Investigators of the Multicenter Study of Hydroxyurea in Sickle Cell Anemia, *N. Engl. J. Med.*, 1995, **332**, 1317–1322.

10 A. N. Schechter and G. P. Rodgers, Sickle Cell Anemia—Basic Research Reaches the Clinic, *N. Engl. J. Med.*, 1995, **332**, 1372–1374, DOI: **10.1056/nejm199505183322010**.

11 W. Y. Gao, A. Cara, R. C. Gallo and F. Lori, Low levels of deoxynucleotides in peripheral blood lymphocytes: a strategy to inhibit human immunodeficiency virus type 1 replication, *Proc. Natl. Acad. Sci.*, 1993, **90**, 8925–8928, DOI: **10.1073/PNAS.90.19.8925**.

12 S. Cortelazzo, G. Finazzi, M. Ruggeri, O. Vestri, M. Galli, F. Rodeghiero and T. Barbui, Hydroxyurea for Patients with Essential Thrombocythemia and a High Risk of Thrombosis, *N. Engl. J. Med.*, 1995, **332**, 1132–1137, DOI: **10.1056/nejm199504273321704**.

13 M. ROSTEN, Hydroxyurea: A New Antimetabolite In The Treatment Of Psoriasis, *Br. J. Dermatol.*, 1971, **85**, 177–181, DOI: **10.1111/j.1365-2133.1971.tb07206.x**.

14 P. B. Donovan, M. E. Kaplan, J. D. Goldberg, I. Tatarsky, Y. Najean, E. B. Silberstein, W. H. Knospe, J. Laszlo, K. Mack, P. D. Berk and L. R. Wasserman, Treatment of polycythemia vera with hydroxyurea, *Am. J. Hematol.*, 1984, **17**, 329–334, DOI: **10.1002/ajh.2830170402**.

15 J. T. Chou, W. T. Beck, T. Khwaja, K. Mayer and E. J. Lien, Synthesis and anticancer activity of novel cyclic N-hydroxyureas, *J. Pharm. Sci.*, 1977, **66**, 1556–1561, DOI: **10.1002/jps.2600661114**.

16 M. S. Aslam, S. Naveed, A. Ahmed, Z. Abbas, I. Gull and M. A. Athar, Side Effects of Chemotherapy in Cancer Patients and Evaluation of Patients Opinion about Starvation Based Differential Chemotherapy, *J. Cancer Ther.*, 2014, **5**, DOI: **10.4236/jct.2014.58089**.

17 M. G. Muktadir, A. Alam, A. A. Piya and S. U. D. Shamim, Exploring the adsorption ability with sensitivity and reactivity of C12-B6N6, C12-Al6N6, and B6N6-Al6N6 heteronanocages towards the cisplatin drug: a DFT, AIM, and COSMO analysis, *RSC Adv.*, 2022, **12**, 29569–29584, DOI: **10.1039/d2ra04011e**.

18 S. U. D. Shamim, M. H. Miah, M. R. Hossain, M. M. Hasan, M. K. Hossain, M. A. Hossain and F. Ahmed, Theoretical investigation of emodin conjugated doped B12N12 nanocage by means of DFT, QTAIM and PCM analysis, *Phys. E*, 2022, **136**, 115027, DOI: **10.1016/j.physe.2021.115027**.

19 A. Soltani, M. T. Baei, E. Tazikeh Lemeski, S. Kaveh and H. Balakheyli, A DFT study of 5-fluorouracil adsorption on the pure and doped BN nanotubes, *J. Phys. Chem. Solids*, 2015, **86**, 57–64, DOI: **10.1016/j.jpcs.2015.06.008**.

20 M. Rakib Hossain, M. Mehade Hasan, S. Ud Daula Shamim, T. Ferdous, M. Abul Hossain and F. Ahmed, First-principles study of the adsorption of chlormethine anticancer drug on C24, B12N12 and B12C6N6 nanocages, *Comput. Theor. Chem.*, 2021, **1197**, 113156, DOI: **10.1016/j.comptc.2021.113156**.

21 H. Zhang, M. Chhowalla and Z. Liu, 2D nanomaterials: Graphene and transition metal dichalcogenides, *Chem. Soc. Rev.*, 2018, **47**, 3015–3017, DOI: **10.1039/c8cs90048e**.

22 S. U. D. Shamim, M. K. Hossain, S. M. Hasan, A. A. Piya, M. S. Rahman, M. A. Hossain and F. Ahmed, Understanding Na-ion adsorption in nitrogen doped graphene oxide anode for rechargeable sodium ion batteries, *Appl. Surf. Sci.*, 2022, **579**, 152147, DOI: **10.1016/j.apsusc.2021.152147**.

23 S. Das, S. Ud, D. Shamim, K. Hossain, F. Ahmed, A. Hossain and M. Obaidur, A novel silicon-doped 2D Ti 2 C MXene monolayer as high capacity stable anode material for lithium ion batteries : Insight from density functional theory study, *Appl. Surf. Sci.*, 2022, **600**, 154173, DOI: **10.1016/j.apsusc.2022.154173**.

24 S. U. D. Shamim, D. Roy, S. Alam, A. A. Piya, M. S. Rahman, M. K. Hossain and F. Ahmed, Doubly doped graphene as gas sensing materials for oxygen-containing gas molecules: A first-principles investigation, *Appl. Surf. Sci.*, 2022, **596**, 153603, DOI: **10.1016/j.apsusc.2022.153603**.

25 S. U. Daula Shamim, M. K. Hossain, S. M. Hasan, A. Hossain and F. Ahmed, Ab initio study of N-doped graphene oxide (NDGO) as a promising anode material for Li-ion rechargeable battery, *Mol. Simul.*, 2020, **46**, 1135–1145, DOI: **10.1080/08927022.2020.1805115**.

26 A. Vaidyanathan, M. Mathew, S. Radhakrishnan, C. S. Rout and B. Chakraborty, Theoretical Insight on the Biosensing Applications of 2D Materials, *J. Phys. Chem. B*, 2020, **124**, 11098–11122, DOI: **10.1021/acs.jpcb.0c08539**.

27 H. L. Guo, X. F. Wang, Q. Y. Qian, F. Bin Wang and X. H. Xia, A green approach to the synthesis of graphene nanosheets, *ACS Nano*, 2009, **3**, 2653–2659, DOI: **10.1021/nn900227d**.

28 Z. Yang, R. Gao, N. Hu, J. Chai, Y. Cheng, L. Zhang, H. Wei, E. S. W. Kong and Y. Zhang, The prospective two-dimensional graphene nanosheets: preparation, functionalization, and applications, *Nano-Micro Lett.*, 2012, DOI: **10.3786/nml.v4i1.p1-9**.

29 S. Alwarappan, A. Erdem, C. Liu and C. Z. Li, Probing the electrochemical properties of graphene nanosheets for biosensing applications, *J. Phys. Chem. C*, 2009, **113**, 8853–8857, DOI: **10.1021/jp9010313**.

30 S. Sattari, M. Adeli, S. Beyranvand and M. Nemati, Functionalized graphene platforms for anticancer drug delivery, *Int. J. Nanomed.*, 2021, 5955–5980, DOI: **10.2147/IJN.S249712**.

31 X. Li, Y. Wang, L. Shi, H. Ma, Y. Zhang, B. Du, D. Wu and Q. Wei, A novel ECL biosensor for the detection of concanavalin A based on glucose functionalized NiCo2S4 nanoparticles-grown on carboxylic graphene as quenching probe, *Biosens. Bioelectron.*, 2017, **96**, 113–120, DOI: **10.1016/j.bios.2017.04.050**.

32 F. N. Xiao, M. Wang, F. Bin Wang and X. H. Xia, Graphene-ruthenium(II) complex composites for sensitive ECL immunosensors, *Small*, 2014, **10**, 706–716, DOI: **10.1002/smll.201301566**.

33 C. I. Wang, W. C. Wu, A. P. Periasamy and H. T. Chang, Sensitive and selective DNA probe based on "turn-on" photoluminescence of C-dots@RGO, *Anal. Bioanal. Chem.*, 2014, **406**, 6917–6923, DOI: **10.1007/s00216-014-7658-2**.

34 J. Liu, L. Cui and D. Losic, Graphene and graphene oxide as new nanocarriers for drug delivery applications, *Acta Biomater.*, 2013, **9**, 9243–9257, DOI: **10.1016/j.actbio.2013.08.016**.

35 S. Bhandary and B. Sanyal, *Graphene-Boron Nitride Composite: A Material with Advanced Functionalities*, IntechOpen, 2012, pp. 1–14.

36 L. Ci, L. Song, C. Jin, D. Jariwala, D. Wu, Y. Li, A. Srivastava, Z. F. Wang, K. Storr, L. Balicas, F. Liu and P. M. Ajayan, Atomic layers of hybridized boron nitride and graphene domains, *Nat. Mater.*, 2010, **9**, 430–435, DOI: **10.1038/nmat2711**.

37 M. Ayoubi-Chianeh and M. Z. Kassaee, Detection of bendamustine anti-cancer drug *via* AlN and Si-doped C nanocone and nanosheet sensors by DFT, *Struct. Chem.*, 2020, **31**, 2041–2050, DOI: **10.1007/s11224-020-01561-5**.

38 S. R. Deepak Arumugam, M. Subramani, R. Durai and A. Sambasivam, Probing the influence of defects and Si-doping in graphene sheet as an efficacious carrier for drug delivery system in gas and aqua phases-Combined DFT and classical MD simulation, *J. Phys. Chem. Solids*, 2023, 111562.

39 H. O. Edet, H. Louis, T. E. Gber, P. S. Idante, T. G. C. Egemonye, P. B. Ashishie, E. E. Oyo-Ita, I. Benjamin and A. S. Adeyinka, Heteroatoms (B, N, S) doped quantum dots as potential drug delivery system for isoniazid: insight from DFT, NCI, and QTAIM, *Heliyon*, 2023, DOI: 10.1016/j.heliyon.2022.e12599.

40 B. Delley, An all-electron numerical method for solving the local density functional for polyatomic molecules, *J. Chem. Phy.*, 1990, **92**, 508–517.

41 B. Delley, From molecules to solids with the DMol3 approach, *J. Chem. Phys.*, 2000, **113**, 7756–7764, DOI: 10.1063/1.1316015.

42 J. P. Perdew, K. Burke and M. Ernzerhof, Generalized gradient approximation made simple, *Phys. Rev. Lett.*, 1996, **77**, 3865–3868, DOI: 10.1103/PhysRevLett.77.3865.

43 S. GRIMME, Semiempirical GGA-Type Density Functional Constructed with a Long-Range Dispersion Correction, *J. Comput. Chem.*, 2006, **32**, 174–182, DOI: 10.1002/jcc.

44 B. Delley, Hardness conserving semilocal pseudopotentials, *Phys. Rev. B: Condens. Matter Mater. Phys.*, 2002, **66**, 155125, DOI: 10.1103/PhysRevB.66.155125.

45 H. P. Zhang, X. G. Luo, H. T. Song, X. Y. Lin, X. Lu and Y. Tang, DFT study of adsorption and dissociation behavior of H$_2$S on Fe-doped graphene, *Appl. Surf. Sci.*, 2014, **317**, 511–516, DOI: 10.1016/j.apsusc.2014.08.141.

46 M. J. Ungerer, C. G. C. E. Van Sittert, D. J. Van Der Westhuizen and H. M. Krieg, Molecular modelling of tantalum penta-halides during hydrolysis and oxidation reactions, *Comput. Theor. Chem.*, 2016, **1090**, 112–119, DOI: 10.1016/j.comptc.2016.06.011.

47 B. Delley, The conductor-like screening model for polymers and surfaces, *Mol. Simul.*, 2006, **32**, 117–123, DOI: 10.1080/08927020600589684.

48 R. G. Pearson, Absolute Electronegativity and Hardness: Applications to Organic Chemistry, *J. Org. Chem.*, 1989, **54**, 1423–1430, DOI: 10.1021/jo00267a034.

49 R. G. P. P. K. Chattaraj, Density functional theory of chemical reactivity, *Chem. Modell.*, 2015, **11**, 151–174, DOI: 10.1039/9781782620112-00151.

50 S. U. D. Shamim, T. Hussain, M. R. Hossian, M. K. Hossain, F. Ahmed, T. Ferdous and M. A. Hossain, A DFT study on the geometrical structures, electronic, and spectroscopic properties of inverse sandwich monocyclic boron nanoclusters ConBm ($n = 1.2$; $m = 6$–$8$), *J. Mol. Model.*, 2020, **26**, 1–17, DOI: 10.1007/s00894-020-04419-z.

51 A. S. Rad, S. S. Shabestari, S. A. Jafari, M. R. Zardoost and A. Mirabi, N-doped graphene as a nanostructure adsorbent for carbon monoxide: DFT calculations, *Mol. Phys.*, 2016, **114**, 1756–1762, DOI: 10.1080/00268976.2016.1145748.

52 R. A. Yossa Kamsi, G. W. Ejuh, Y. Tadjouteu Assatse, C. A. Njeumen, F. Tchoffo and J. M. B. Ndjaka, Computational study of reactivity and solubility of Rubescin D and E molecules in gas phase and in solvent media using Hartree-Fock and DFT methods, *J. Mol. Model.*, 2019, DOI: 10.1016/j.cjph.2019.04.020.

53 M. Shahabi and H. Raissi, Investigation of the solvent effect, molecular structure, electronic properties and adsorption mechanism of Tegafur anticancer drug on graphene nanosheet surface as drug delivery system by molecular dynamics simulation and density functional approach, *J. Incl. Phenom. Macrocycl. Chem.*, 2017, **88**, 159–169, DOI: 10.1007/s10847-017-0713-9.

54 S. N. Ema, M. A. Khaleque, A. Ghosh, A. A. Piya, U. Habiba and S. U. D. Shamim, Surface adsorption of nitrosourea on pristine and doped (Al, Ga and In) boron nitride nanosheets as anticancer drug carriers: The DFT and COSMO insights, *RSC Adv.*, 2021, **11**, 36866–36883, DOI: 10.1039/d1ra07555a.

55 A. A. Piya, S. U. D. Shamim, M. N. Uddin, K. N. Munny, A. Alam, M. K. Hossain and F. Ahmed, Adsorption behavior of cisplatin anticancer drug on the pristine, Al-and Ga-doped BN nanosheets: A comparative DFT study, *Comput. Theor. Chem.*, 2021, **1200**, 113241, DOI: 10.1016/j.comptc.2021.113241.

56 J. Mawwa, S. U. D. Shamim, S. Khanom, M. K. Hossain and F. Ahmed, In-plane graphene/boron nitride heterostructures and their potential application as toxic gas sensors, *RSC Adv.*, 2021, **11**, 32810–32823, DOI: 10.1039/d1ra06304a.

57 T. Ahmed, M. Rahman, R. Islam, A. A. Piya. and S. U. D. Shamim, Unravelling the adsorption performance of BN, AlN, GaN and InN 2D nanosheets towards the ciclopirox, 5-fluorouracil and nitrosourea for anticancer drug delivery, *Comput. Theor. Chem.*, 2022, **1214**, 113797.

58 A. A. Piya, T. Ahmed, M. Abdul Khaleque, K. Ahmed and S. U. D Shamim, Trivalent and pentavalent atoms doped boron nitride nanosheets as Favipiravir drug carriers for the treatment of COVID-19 using computational approaches, *Comput. Theor. Chem.*, 2022, **1217**, 113902, DOI: 10.1016/J.COMPTC.2022.113902.

59 R. Ziraoui, H. Meghraoui, M. El Gouri, M. Rafik and A. Elharfi, Synthesis and physico chemical study of a new hexa and tetra functional epoxy materials based on bis -para-terephthalylidene phosphoric ester, *J. Mol. Model.*, 2010, **1**, 213–218.

60 P. K. Chattaraj, U. Sarkar and D. R. Roy, Electrophilicity index, *Chem. Rev.*, 2006, **106**, 2065–2091, DOI: 10.1021/cr040109f.